Cellular/Molecular

Gamma Oscillations and Spontaneous Network Activity in the Hippocampus Are Highly Sensitive to Decreases in pO_2 and Concomitant Changes in Mitochondrial Redox State

Christine Huchzermeyer, Klaus Albus, Hans-Jürgen Gabriel, Jakub Otáhal, Nando Taubenberger, Uwe Heinemann, Richard Kovács, and Oliver Kann

Institute for Neurophysiology, Charité-Universitätsmedizin Berlin, 10117 Berlin, Germany

Gamma oscillations have been implicated in higher cognitive processes and might critically depend on proper mitochondrial function. Using electrophysiology, oxygen sensor microelectrode, and imaging techniques, we investigated the interactions of neuronal activity, interstitial pO_2, and mitochondrial redox state [NAD(P)H and FAD (flavin adenine dinucleotide) fluorescence] in the CA3 subfield of organotypic hippocampal slice cultures. We find that gamma oscillations and spontaneous network activity decrease significantly at pO_2 levels that do not affect neuronal population responses as elicited by moderate electrical stimuli. Moreover, pO_2 and mitochondrial redox states are tightly coupled, and electrical stimuli reveal transient alterations of redox responses when pO_2 decreases within the normoxic range. Finally, evoked redox responses are distinct in somatic and synaptic neuronal compartments and show different sensitivity to changes in pO_2. We conclude that the threshold of interstitial pO_2 for robust CA3 network activities and required mitochondrial function is clearly above the "critical" value, which causes spreading depression as a result of generalized energy failure. Our study highlights the importance of a functional understanding of mitochondria and their implications on activities of individual neurons and neuronal networks.

Key words: **gamma; local field potential; mitochondria; NADPH; potassium concentration; [K]; tissue oxygen**

Introduction

Fast neuronal network oscillations in the gamma range (~30–80 Hz) occur in various brain regions and are thought to provide a temporal structure for higher brain functions, such as sensory processing, memory formation, and perhaps consciousness (Buzsáki and Draguhn, 2004; Bartos et al., 2007). Conversely, disturbances of gamma oscillations might underlie cognitive dysfunction and psychiatric disorders (Whittington et al., 2000; Cho et al., 2006). Gamma oscillations are also prevalent in the hippocampus, where they have been implicated in encoding and retrieval of memory traces (Bragin et al., 1995; Lisman and Idiart, 1995; Montgomery and Buzsáki, 2007). In the hippocampal CA3 subfield, gamma oscillations arise from the precise interplay of action potential firing of excitatory glutamatergic pyramidal neurons and fast inhibitory GABAergic interneurons (Bartos et al., 2007). As a consequence, alternating pairs of current sinks and sources occur in stratum pyramidale and stratum radiatum (Csicsvari et al., 2003; Mann et al., 2005), which require enhanced activation of Na^+/K^+-ATPases to restore ionic gradients and to maintain excitability (Attwell and Iadecola, 2002). Thus, we hypothesized that gamma oscillations might critically depend on sufficient neuronal ATP supply. This is supported by a report showing that synchronized gamma oscillations and hemodynamic signals tightly correlate *in vivo* (Niessing et al., 2005). Strikingly, the relationships between gamma oscillations and energy metabolism have been scarcely explored.

Most of the ATP that is used in the brain is produced by oxidative phosphorylation in mitochondria, which requires sufficient glucose and oxygen availability (Erecinska and Silver, 2001). Mitochondria show a significant and yet largely unexplained heterogeneity in number, size, distribution, and enzyme activity in neuronal cell types (Wong-Riley, 1989; Waagepetersen et al., 1999; Popov et al., 2005), and they rapidly counterbalance local ATP consumption mainly in response to changes in substrates like ADP/ATP ratio and intracellular Ca^{2+} (Kann and Kovács, 2007). Moreover, critical steps in the metabolism of neurotransmitters glutamate and GABA are located in the mitochondrial tricarboxylic acid (TCA) cycle (Waagepetersen et al., 1999).

The present study was designed to investigate the oxygen and energy demands of gamma oscillations, which is of central importance to understand both the physiological determinants of higher brain functions and their remarkable vulnerability during pathological processes. Therefore, we explored the sensitivity of gamma oscillations and spontaneous network activity in CA3 to

Received Sept. 7, 2007; revised Dec. 18, 2007; accepted Dec. 18, 2007.

This work was supported by Deutsche Forschungsgemeinschaft Grants SFB-665 (O.K.) and SFB-507 (O.K., U.H.), and by "Stiftung zur Förderung der Erforschung von Ersatz- und Ergänzungsmethoden zur Einschränkung von Tierversuchen" (K.A.). We thank Kristin Fröhlich for excellent technical assistance.

Correspondence should be addressed to Dr. Oliver Kann, Neuronal Mitochondria Research Group, Institute for Neurophysiology, Charité-Universitätsmedizin Berlin, Tucholskystrasse 2, 10117 Berlin, Germany. E-mail: oliver.kann@charite.de.

J. Otáhal's present address: Department of Developmental Epileptology, Institute of Physiology, Academy of Sciences, Videnska 1083, 14220 Prague 4, Czech Republic.

DOI:10.1523/JNEUROSCI.4105-07.2008

 0270-6474/08/281153-10$15.00/0

changes in interstitial partial oxygen pressure (pO_2) and mitochondrial redox state. For comparison, we also determined the sensitivity of neuronal population responses as elicited by moderate electrical stimuli to changes in pO_2 and redox state. We used organotypic hippocampal slice cultures (180–210 μm thickness) because of shorter diffusion distances for O_2 and substrates from the ambient media compared with acute slices, and adaptation to normal atmosphere, which allows a wide range of changes in tissue oxygenation without occurrence of pathological activity (Kann and Kovács, 2007). Gamma oscillations were evoked by activation of acetylcholine (ACh) receptors, which mimics cholinergic input from the septum (Fischer et al., 2002). Cholinergically evoked oscillations share many features with physiological intrahippocampal gamma oscillations *in vivo* (Fisahn et al., 1998; Csicsvari et al., 2003) and require both excitation and fast inhibition (Bartos et al., 2007).

Materials and Methods

Tissue culture. Organotypic hippocampal slice cultures were prepared as described previously (Kann et al., 2003). In brief, hippocampal slices (400 μm) were cut from 7- to 9-d-old Wistar rat brains under sterile conditions in cold minimal essential medium (MEM; Invitrogen, Karlsruhe, Germany) saturated with 95% O_2 and 5% CO_2. Slices were maintained on a biomembrane surface (Millipore, Eschborn, Germany) between culture medium [50% MEM, 25% HBSS (Sigma, Taufkirchen, Germany), 25% horse serum (Invitrogen), and 2 mM L-glutamine at pH 7.3] and humidified atmosphere (5% CO_2, 36.5°C) in an incubator (Unitherm 150; UniEquip, Martinsried, Germany). Half of the medium was replaced three times per week. Slice cultures were used for experiments between 7 and 17 d *in vitro* (residual thickness of 180–210 μm). Rats were housed, cared for, and killed in accordance with the recommendations of the European Commission and the Berlin Animal Ethics Committee (T 0291/04).

Solutions and recordings. Slice cultures on excised membranes were maintained in the recording chamber with saturated (20 or 95% O_2, 5% CO_2) artificial CSF (ACSF) that contained (in mM) 129 NaCl, 3 KCl, 1.25 NaH_2PO_4, 1.8 $MgSO_4$, 1.6 $CaCl_2$, 21 $NaHCO_3$, and 10 glucose, pH 7.3. Components of ACSF and ACh were from Sigma, and physostigmine was from Tocris Bioscience (Bristol, UK) (distributed by Biotrend, Köln, Germany). Experiments were performed at 34 ± 1°C in an interface chamber or at 24–26°C under submerged recording conditions with ACSF flow rates of 2 and 5 ml/min, respectively. Fluorescence and pO_2 recordings were made in submerged recording chambers mounted on Axioskop (Zeiss, Jena, Germany) and BX51WI upright microscopes (Olympus, Hamburg, Germany) using 20× [0.5 numerical aperture (NA)] and 10× (0.3 NA) water-immersion objectives or a 4× objective (0.28 NA) with a water cap. For recordings of multiunit activity and gamma oscillations, self-made interface recording chambers were used (Stenkamp et al., 2001; Pomper et al., 2006). Recording microelectrodes (K^+-sensitive/local field potential, O_2-sensitive) were placed in stratum pyramidale of the CA3 subfield, and a bipolar stimulation electrode (tungsten filament, tip diameter of ~10 μm) was positioned close to the dentate gyrus to activate fiber tracts to CA3. Electrical stimulation was made with either a single stimulus or trains of stimuli (0.1 ms duration, 10 s at 20 Hz or 1 s at 100 Hz).

Electrophysiology. Multiunit activity was recorded with low-impedance tungsten in glass microelectrodes. Single units were discriminated with a template-matching algorithm (Gaedicke and Albus, 1995). DC-coupled recordings of local field potentials and changes in extracellular potassium concentration ($[K^+]_o$) were performed with double-barreled reference and K^+-sensitive microelectrodes (Heinemann and Arens, 1992). In brief, electrodes were pulled from double-barreled theta glass (Science Products, Hofheim, Germany). The reference barrel was filled with 154 mM NaCl solution, the ion-sensitive barrel with K^+ ionophore I cocktail A (60031; Fluka Chemie, Buchs, Switzerland) and 100 mM KCl. K^+-sensitive microelectrodes with a sensitivity of 59 ± 2 mV to a 10-fold increase in K^+ concentration were used for experiments. The amplifier was equipped with negative capacitance feedback control, which permitted recordings of changes in $[K^+]_o$ with time constants of 50–200 ms. Changes in voltage were digitized at 10 Hz using FeliX software (Photon Technology Instruments, Wedel, Germany) or at 5 kHz (local field potentials, 1 kHz low-pass filter) and 20 kHz (multiunits, 5 kHz low-pass filter) using CED 1401 interface and Spike 2 software (Cambridge Electronic Design, Cambridge, UK).

Oxygen sensor microelectrode. An oxygen sensor microelectrode (tip diameter of 10 μm; 737GC; Diamond General Development, Ann Arbor, MI) was used to continuously measure changes in pO_2. This new type of modified polarographic Clark electrodes consists of a glass-insulated Ag/AgCl reference anode and a guard cathode with the advantages of low sensitivity to motion artifact, a time constant of <1 s (0–90%), minimal interaction with tissue, and low O_2 consumption (Foster et al., 2005; Pomper et al., 2006; Takano et al., 2007). For polarization, the electrode was connected to a picoammeter and the tip was maintained in nongassed ACSF overnight, which resulted in a stable current readout. Before and after each experiment, the electrode was calibrated by generating a three-point calibration curve in ACSF saturated with 100% N_2, 20% O_2 (5% CO_2, 75% N_2), or 95% O_2 (5% CO_2) at stable temperature, which revealed a linear relationship between current readout and pO_2. For experiments, the electrode was connected to a polarographic amplifier (chemical microsensor II; Diamond General Development) and placed close to the K^+-sensitive/field potential recording electrode in CA3. Changes in voltage from both electrodes were low-pass filtered and simultaneously digitized at 1 kHz (pO_2) and 5 kHz (CED 1401 interface).

Fluorescence recordings of NAD(P)H and FAD. NAD(P)H and flavin adenine dinucleotide (FAD) were excited at 360 ± 15 nm and 490 ± 10 nm, respectively. Recordings were made with a monochromator system (Photon Technology Instruments) or an epifluorescence illumination system (Olympus Cell∧R) that combines a fast driven excitation filter wheel and a triple band filter, allowing excitation of NAD(P)H and FAD with a delay of 130 ms. NAD(P)H and FAD fluorescence images (emission at 460 ± 10 nm and 530 ± 10 nm, respectively) were recorded at 0.5 Hz using a CCD camera (ORCA-ER; Hamamatsu Photonics, Hamamatsu City, Japan). Fast NAD(P)H fluorescence recordings were made at 10 Hz using photomultiplier-based microfluorimetry (Seefelder Messtechnik, Seefeld, Germany) and FeliX software (Photon Technology Instruments). Because the emission spectra of NADH and NADPH overlap, NAD(P)H indicates that the recorded fluorescence might have originated from either one or both (Schuchmann et al., 2001). Changes in light transmittance were recorded with the same CCD camera settings as used for fluorescence recordings and by illuminating slice cultures with the standard halogen microscope lamp underneath the recording chamber (Buchheim et al., 2002). Changes in NAD(P)H and FAD fluorescence are presented as changes in $\%\Delta F/F_0$, where F_0 is the averaged fluorescence of a 20 s period before stimulation of the tissue.

Calculations and statistics. To translate the recorded potential values (mV) in $[K^+]_o$, a modified Nernst equation was used (Heinemann and Arens, 1992; Kann et al., 2003): $\log[\mathrm{Ion}]_1 = E_M \times (s \times v)^{-1} + \log[\mathrm{Ion}]_o$, with E_M, recorded potential; s, electrode slope obtained at calibration; v, valence of the specific ion; $[\mathrm{Ion}]_o$, ion concentration at rest; and $[\mathrm{Ion}]_1$, ion concentration during activation.

Power spectra of fast network oscillations were calculated by fast Fourier transformation (Hanning window, FFT size 1024) for three data segments of 60 s each: (1) at 95% O_2 oxygenation (control condition), (2) after 2 min at 20% O_2, and (3) after 2 min at 95% O_2 (reoxygenation). For comparison of power spectra at 20% O_2 and reoxygenation, the sum of the power of the bins from 30 to 80 Hz was calculated and normalized to the control condition. Data are reported as mean ± SE and are derived from at least three slice culture preparations per experimental group. Statistical significance ($p < 0.05$) was determined using Student's t tests and ANOVA (Friedman's test and Dunn's *post hoc* test). Calculations and figures were made using Spike 2 (Cambridge Electronic Design), Clampfit 9 (Molecular Devices, Union City, CA), Origin (Microcal Software, Northampton, MA) and CorelDRAW (Corel, Ottawa, Ontario, Canada).

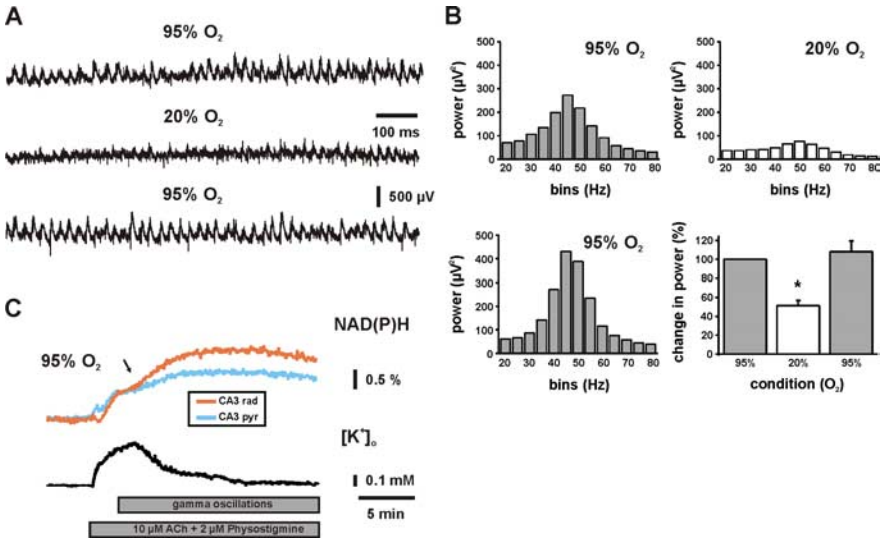

Figure 1. Effects of tissue oxygenation on gamma oscillations and associated mitochondrial redox responses in CA3. ***A***, Local field potentials were recorded in stratum pyramidale, and ACh (10 μM) was continuously applied in the presence of cholinesterase inhibitor physostigmine (2 μM) to evoke robust and persistent gamma oscillations. ***B***, From recordings and conditions as illustrated in ***A***, power spectra were calculated from data segments of 60 s. In the histogram, the gamma band power (30–80 Hz) is significantly reduced at 20% O_2 ($p < 0.001$; $n = 15$). ***C***, Simultaneous recordings of NAD(P)H fluorescence in stratum radiatum (orange) and pyramidale (light blue) as well as $[K^+]_o$ (black) and local field potentials (data not shown) in stratum pyramidale were made during application of ACh (10 μM; bottom gray bar). Initially, the increase in $[K^+]_o$ was associated with a biphasic NAD(P)H fluorescence transient (dip and overshoot component), which transformed into a persistent NAD(P)H elevation (black arrow) when gamma oscillations were fully established (illustrated as top gray bar). Note that persistent NAD(P)H elevations were significantly larger in stratum radiatum. Figure 5*A* illustrates the selection of regions of interest for fluorescence imaging. *$p < 0.05$.

Results

Neuronal activity and tissue oxygenation

Fast network oscillations as evoked by bath application of ACh (10 μM) in the presence of cholinesterase inhibitor physostigmine (2 μM) were persistent and characterized by high power in the gamma range (30–80 Hz) at 95% O_2 under both interface and submerged recording conditions (Fig. 1). The highest power was observed in bins of 45–50 Hz (Fig. 1*B*) and 35–40 Hz ($n = 8$; data not shown), respectively. This slight difference was likely a result of the lower temperature under submerged recording conditions (see Materials and Methods). A rapid switch to 20% O_2 significantly reduced the power of gamma oscillations within 1–2 min, clearly indicating a high sensitivity to decreases in interstitial pO_2. Reoxygenation with 95% O_2 resulted in full recovery (Fig. 1*A*, traces, and corresponding power spectra in 1*B*). In some experiments, gamma oscillations showed a higher power within the first 2–5 min during reoxygenation (Fig. 1*B*, lower power spectrum). However, this effect was not statistically significant when compared with the 95% O_2 control condition ($n = 15$; $p = 0.49$). In another set of experiments, we applied high-frequency stimulation (100 Hz, 1 s) to elicit gamma oscillations in CA1, which persisted for 3 s after the stimuli (data not shown). At 20% O_2, the power of these gamma oscillations decreased significantly by 42 ± 6% ($n = 8$; $p < 0.01$). The effect was completely reversible at 95% O_2 reoxygenation and indicated that our finding was not restricted to the model of cholinergically evoked gamma oscillations and the CA3 subfield.

To test whether the sensitivity to decreases in pO_2 was specific for gamma oscillations, we investigated the effects of tissue oxygenation on spontaneous network activity by applying multiunit recordings in CA3. We found that spontaneous network activity decreased within minutes at 20% O_2 as well (Fig. 2*A*). To get further insight into the characteristics of the neurons that were affected, we performed single-unit discrimination (Gaedicke and Albus, 1995). During 60 min of stable recordings at 95% O_2, single units were identified ($n = 69$) and classified according to spike rates in three groups, showing <2, 2–5, and >5 spikes per second, respectively (Fig. 2*B*). At 20% O_2, the spike rates decreased in all groups and reversed completely during reoxygenation. The strongest spike reduction occurred after 30–60 min at 20% O_2.

In sharp contrast to network activities, shape and amplitude (1.7 ± 0.1 mV vs 1.8 ± 0.1 mV; $n = 10$; $p = 0.49$) of local field potential responses as elicited by moderate electrical stimuli were unaffected by changes in tissue oxygenation (Fig. 2*C*). Moreover, amplitudes and kinetics of transient increases in $[K^+]_o$, which were elicited by stimulus trains (10 s, 20 Hz), did not differ at 95 and 20% O_2 (Figs. 3*B*,*E*, 4*A*,*B*, 5*B*). We note that electrical stimulation was moderate because (1) local field potential responses were elicited with 70–80% of the intensity required for maximal responses, and (2) $[K^+]_o$ transients were evoked of <2.5 mM, which corresponds to the physiological range *in vivo* (Heinemann et al., 1990; Amzica and Steriade, 2000). These data indicated that specifically gamma oscillations and spontaneous network activity were highly sensitive to decreases in pO_2. We further hypothesized that this might have been mediated by limitations of mitochondrial function at 20% O_2.

To quantify interstitial pO_2 levels, O_2 consumption, and changes in mitochondrial redox state under both oxygenation conditions, we used an oxygen sensor microelectrode and fluorescence recordings of NAD(P)H and FAD. Because of the high O_2 sensitivity of gamma oscillations and the observation that gamma oscillations elicited only slow elevations in NAD(P)H fluorescence at 95% O_2 (Fig. 1*C*) (see below), this type of activity was not useful to get insight into the postulated limitations of mitochondrial function at 20% O_2. Therefore, we applied electrical stimulus trains (10 s, 20 Hz) as another experimental tool to trigger temporally defined neuronal activation and associated mitochondrial redox responses [NAD(P)H and FAD transients] in CA3. Such stimulus trains are well tolerated by hippocampal tissue (Schuchmann et al., 2001; Foster et al., 2005; Kann et al., 2005), and we recently demonstrated that there are tight positive correlations between neuronal activation and redox responses over a wide range of stimulus intensities and frequencies (5, 20, 100 Hz) (Kann et al., 2003).

Quantification of interstitial pO_2

The Clark-style microelectrode with low O_2 consumption has been commonly used to monitor interstitial pO_2 levels even under hypoxic conditions in hippocampal slice preparations (Foster et al., 2005; Pomper et al., 2006) and *in vivo* (Takano et al., 2007). We determined a pO_2 of 578 ± 17 mmHg ($n = 9$) at the surface of the slices (Fig. 3*C*), which was considerably lower as calculated and calibrated for ACSF saturated with 95% O_2 at 24°C in the

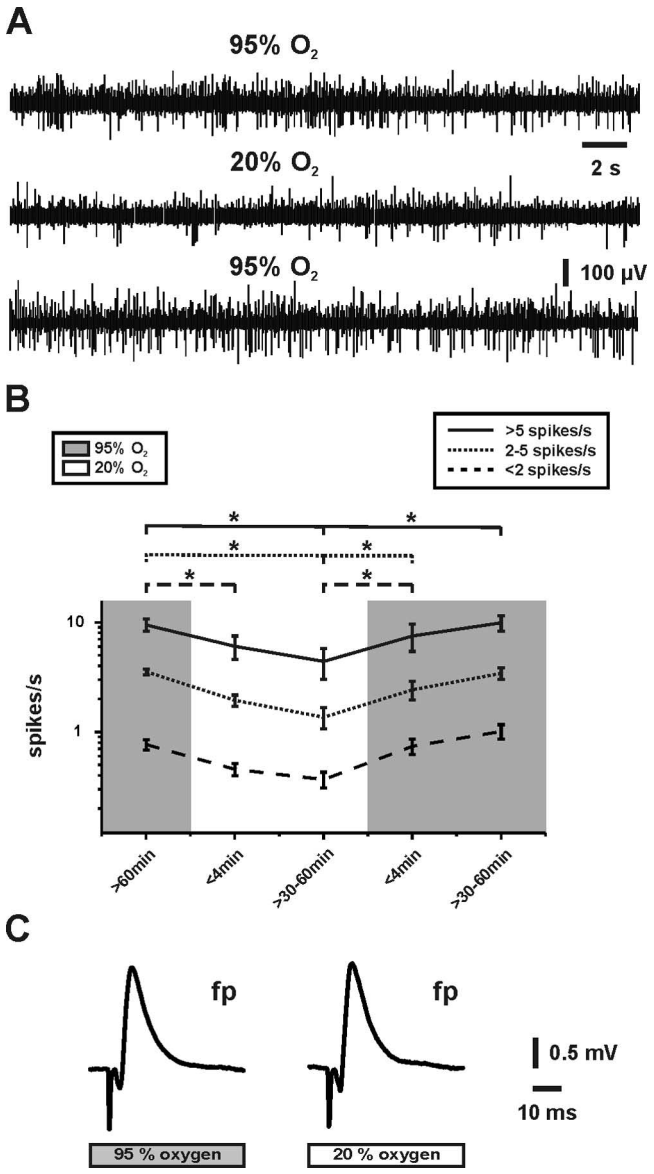

Figure 2. Effects of tissue oxygenation on spontaneous network activity and evoked local field potential responses in CA3. ***A***, Multiunit activity was recorded continuously in stratum pyramidale, and oxygenation was changed according to the protocol as illustrated in ***B***. ***B***, Applying single-unit discrimination in recording periods of 180 s, single units were classified in three groups according to their spike rates (spikes/s), which revealed a distribution of 10% (solid line), 22% (dotted line), and 68% (dashed line) (from $n = 69$) at 95% O_2 (gray background). Note that the spike rates declined in all groups at 20% O_2 (white background), which was reversible. ***C***, After 15 min under the respective oxygenation condition, local field potential responses (fp) were evoked orthodromically by application of single electrical stimuli to the fiber tracts from dentate gyrus to CA3. Note that there were no differences in shape and amplitude (see Results) of the responses. $^*p < 0.05$.

storage container (694 mmHg). The difference reflected a loss of ~15% of O_2 saturation because of diffusion from ACSF to the ambient normal atmosphere. There was no discrepancy at 20% O_2 because the measured pO_2 of 148 ± 2 mmHg ($n = 9$) closely matched the estimation for 24°C (146 mmHg). In a depth of 100 µm, the pO_2 baselines were considerably lower (Fig. 3*A*,*C*), indicating substantial O_2 consumption as a result of metabolic demands of active neurons and glial cells (Attwell and Iadecola, 2002; Thompson et al., 2003). When comparing 95 and 20% O_2 conditions, the pO_2 in the slice core dropped from 472 ± 11 to 51 ± 4 mmHg ($n = 18$) (Fig. 3*A*,*C*).

During stimulus trains, the pO_2 rapidly decreased (Fig. 3*A*,*B*). These pO_2 transients reflected enhanced O_2 consumption of the mitochondrial electron transport chain (Foster et al., 2005; Hayakawa et al., 2005). At 95% O_2, the lowest pO_2 was 293 mmHg and thus clearly hyperoxic. At 20% O_2, the pO_2 decreased on average to 24.9 ± 2 mmHg ($n = 18$) (Fig. 3*C*,*E*). Although stimulus trains evoked virtually the same transient increases in $[K^+]_o$ under both oxygenation conditions, amplitudes of pO_2 transients (Fig. 3*B*,*E*) and integrals as determined from onset to nadir of pO_2 transients were significantly reduced at 20% O_2 (reduction to 63 ± 8% as normalized to 95% O_2 condition; $n = 18$; $p < 0.01$). Moreover, pO_2 transients were more variable at 95% O_2 and reached amplitudes of up to 106 mmHg. These observations might indicate a significant reduction in O_2 availability during stimulation at lower pO_2. The rise times of pO_2 transients during stimulation were not significantly different under both oxygenation conditions. In contrast, the decay time was significantly prolonged at 20% O_2 (Fig. 3*D*), which was suggestive for a reduced O_2 diffusion gradient from the surface to slice core. The data indicate that during network activities and electrically evoked neuronal activation, interstitial pO_2 values in the slice core were hyperoxic at 95% O_2 and, according to *in vivo* data (Rolett et al., 2000; Erecinska and Silver, 2001), in the normoxic range at 20% O_2.

Changes in mitochondrial redox state

Changes in NAD(P)H and FAD fluorescence intensity primarily reflect changes in mitochondrial redox state, in particular in brain slice preparations in which artifacts resulting from adaptations in blood flow are absent (Schuchmann et al., 2001; Kann et al., 2003; Brennan et al., 2006). We note that FAD fluorescence is more specific for mitochondria (Scholz et al., 1969; Kunz and Kunz, 1985; Huang et al., 2002). Switching from 95 to 20% O_2 resulted in substantial elevation of NAD(P)H fluorescence baseline (8.8 ± 1.9%; $n = 5$) (Fig. 4*A*), which was reversible. The effect was enhanced during hypoxic conditions (95% N_2 and 5% CO_2) (data not shown). Such NAD(P)H elevations indicate less oxidation of the dinucleotide pool by the mitochondrial electron transport chain (Mayevsky and Chance, 1975; Foster et al., 2005). Less oxidation was also observed for FAD at 20% O_2 (data not shown). The time constants of NAD(P)H baseline elevation (163 ± 27 s; $n = 5$) and pO_2 baseline decrease (112 ± 7 s; $n = 4$) were not significantly different ($p = 0.18$), indicating a tight correlation between changes in mitochondrial redox state and pO_2 (Figs. 3*A*, 4*A*).

Stimulus trains evoked NAD(P)H fluorescence transients that were characterized by an initial "dip" and a sustained "overshoot" component (Fig. 4*A*), mainly reflecting changes in NAD(P)H oxidation (Kann and Kovács, 2007). Such biphasic NAD(P)H transients have been reported in different brain slice preparations (Lipton, 1973a; Kann et al., 2003; Shuttleworth et al., 2003; Foster et al., 2005). Nevertheless, amplitude and kinetics of NAD(P)H transients differed markedly under both oxygenation conditions. At 20% O_2, the dip component indicating enhanced NAD(P)H oxidation already terminated during stimulus trains of 10 s (Fig. 4*A*), which was also reflected by significantly reduced rise and decay times of the dip (Fig. 4*C*). Taking both, time to peak of the dip component and our data from interstitial pO_2 recordings at 20% O_2 (Fig. 3) into account, we estimated a threshold of 41 ± 5 mmHg ($n = 18$) in the slice core for a transient limitation of mitochondrial oxidation. Overall, the amplitudes of the dip component did not differ under both oxygenation conditions and when fluorescence was recorded as the sum

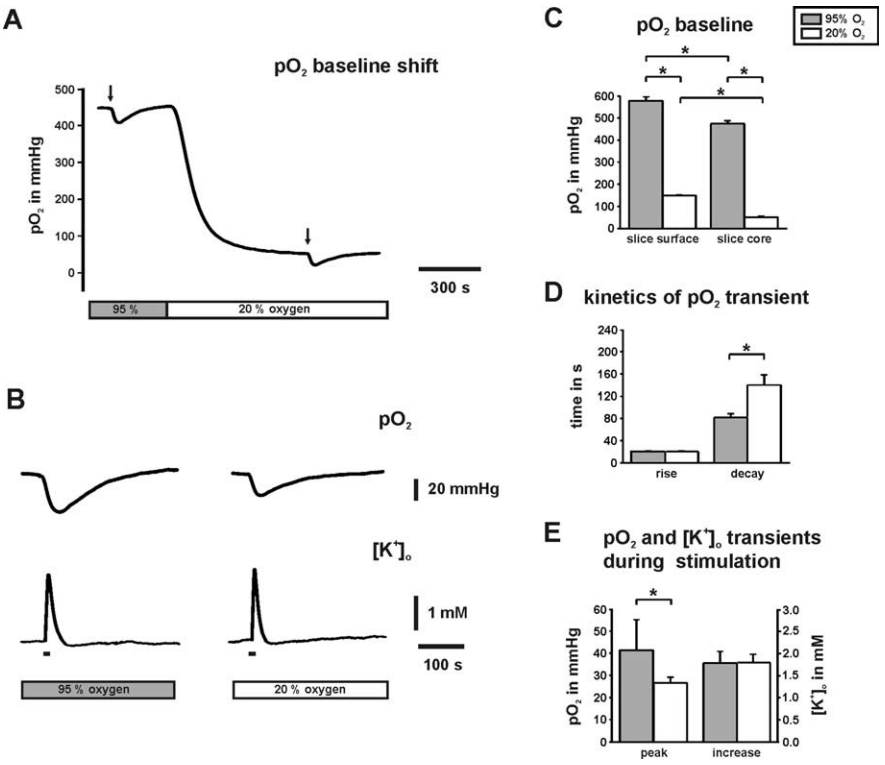

Figure 3. Absolute values of interstitial pO_2 in CA3. The oxygen sensor microelectrode was positioned in stratum pyramidale and the pO_2 was continuously measured. Note that "95% O_2" (gray bars) and "20% O_2" (white bars) refer to saturation levels of ACSF in the storage container. ***A***, The pO_2 baseline shift was measured in the slice core (100 μm depth). Each small pO_2 transient corresponds to enhanced O_2 consumption during neuronal activation as evoked by identical electrical stimulus trains (10 s, 20 Hz; black arrows) to the fiber tracts from dentate gyrus to CA3. ***B***, Traces on an expanded time scale illustrate that pO_2 transients were smaller at 20% O_2, although transient increases in $[K^+]_o$ were similar. ***C***, Histograms summarizing pO_2 baseline values that were determined at the surface ($n = 9$) and in the core ($n = 18$) of slice cultures. Note the significantly smaller pO_2 values in the slice core under both oxygenation conditions. ***D***, Rise and decay times of pO_2 transients during stimulation are given for the 10–90% interval ($n = 18$). Note the significantly slower decay time at 20% O_2. ***E***, pO_2 transients during stimulus trains were significantly smaller at 20% O_2 ($n = 18$). Note that there is no difference in the amplitudes of $[K^+]_o$ transients ($n = 18$), indicating virtually the same degree of neuronal activation under both O_2 conditions. $^*p < 0.05$.

of fluorescence from stratum pyramidale and stratum radiatum using photomultiplier-based microfluorimetry. In contrast, amplitudes of the overshoot were significantly larger at 20% O_2 (Fig. 4*C*). Virtually the same amplitudes (1.56 ± 0.1 mM vs 1.47 ± 0.2 mM; $n = 8$; $p = 0.67$) and kinetics of $[K^+]_o$ transients during identical stimulus trains (Fig. 4*A*,*B*) excluded that the differences in amplitude and kinetics of NAD(P)H transients were caused by less neuronal activation at 20% O_2. At 95% O_2, the dip component was not unlimited because extended stimulus trains of 20, 30, 40 (data not shown), and 60 s at 10 Hz (Fig. 4*A*) revealed a maximal time to the negative peak of 13.7 ± 1 s ($n = 16$). However, this value very likely reflected a transient exhaustion of neurotransmission because increases in $[K^+]_o$ also reached a maximum after 13 ± 2 s ($n = 6$). The data demonstrate that mitochondrial redox state and pO_2 are tightly coupled over a wide range of tissue oxygenation levels and that transient alterations of evoked mitochondrial redox responses [NAD(P)H and FAD transients] occur at pO_2 levels <41 ± 5 mmHg in the slice core.

Because of mitochondrial heterogeneity and diverse local energy demands in neurons (Wong-Riley, 1989; Attwell and Iadecola, 2002; Popov et al., 2005), and indications that the layers in hippocampal slices express different shapes of NAD(P)H transients (Shuttleworth et al., 2003), we applied CCD camera-based imaging to study layer specific differences between stratum pyramidale and stratum radiatum (Fig. 5*A*). At 95% O_2, the amplitudes of dip and overshoot were significantly larger in stratum radiatum, where the stimulated fiber tracts terminate on the dendrites of CA3 neurons (Fig. 5*B*,*C*). Interestingly, the effect of 20% O_2 on amplitudes of dip and overshoot was also most prominent in stratum radiatum, likely indicating a higher O_2 sensitivity of the synaptic compartment. The effects of tissue oxygenation were also evident for stimulus-evoked FAD fluorescence transients (Fig. 5*B*,*D*), and thus substantiated our finding of a transient limitation of oxidation at 20% O_2 in mitochondria. FAD transients were inverse in shape (peak and undershoot) because of different fluorescence properties of flavin adenine dinucleotides (Shuttleworth et al., 2003; Kann and Kovács, 2007). To exclude that the regional differences in NAD(P)H and FAD fluorescence transients were caused by regional differences in light scattering of the tissue during electrical stimulation (Lipton, 1973b), we compared changes in light transmittance during stimulus trains (10 s, 20 Hz) in CA3 by evoking $[K^+]_o$ transients in the range of 1.6–2.2 mM ($n = 9$). Indeed, changes in light transmittance did not differ in both compartments (the values in stratum radiatum were 97 ± 6% of the values in stratum pyramidale; $n = 9$; $p = 0.68$). The tight correlation between changes in mitochondrial redox state and pO_2 was underscored by overlaying traces of NAD(P)H and pO_2 transients under both oxygenation conditions (Fig. 5*E*) as well as by the fact that decay time constants of NAD(P)H overshoot and pO_2 transient were not significantly different (Fig. 5*F*).

Regional differences of NAD(P)H and FAD fluorescence transients were confirmed when exploring the effects of cholinergically evoked gamma oscillations on mitochondrial redox state at 95% O_2 (Fig. 1*C*). In fact, gamma oscillations elicited long-lasting NAD(P)H elevations that were significantly larger in stratum radiatum (1.87 ± 0.1% vs 1.26 ± 0.1%; $n = 8$; $p < 0.01$). In these experiments, ACh application initially evoked increases in $[K^+]_o$ with a peak of 0.39 ± 0.05 mM, which was associated with a biphasic NAD(P)H transient, and a steady-state $[K^+]_o$ level of 0.06 ± 0.02 mM after >15 min ($n = 8$). Long-lasting NAD(P)H elevations emerged slowly when persistent gamma oscillations were fully established at 118 ± 12 s ($n = 8$) after start of ACh application and on top of the initial biphasic NAD(P)H transient (Fig. 1*C*, black arrow). Interestingly, this experiment also showed that gamma oscillations caused more reduction of nicotinamide adenine dinucleotide pool despite hyperoxic pO_2 levels (Fig. 3). The data demonstrate that evoked mitochondrial redox responses differ in somatic and synaptic neuronal compartments.

Discussion

We addressed the oxygen and energy demands of gamma oscillations by exploring the interactions of different types of neuronal activity, interstitial pO_2, and mitochondrial redox state in the

CA3 subfield. Our main findings are (1) gamma oscillations and spontaneous network activity decrease significantly at pO_2 levels that do not affect neuronal population responses as elicited by moderate electrical stimuli, (2) pO_2 and mitochondrial redox states are tightly coupled, (3) electrical stimuli reveal transient alterations of redox responses when pO_2 decreases within the normoxic range, and (4) redox responses as evoked in somatic and synaptic neuronal compartments show different sensitivity to changes in pO_2. We have to emphasize that our investigations were made in the absence of anesthetics and that evoked neuronal activity was within the physiological range.

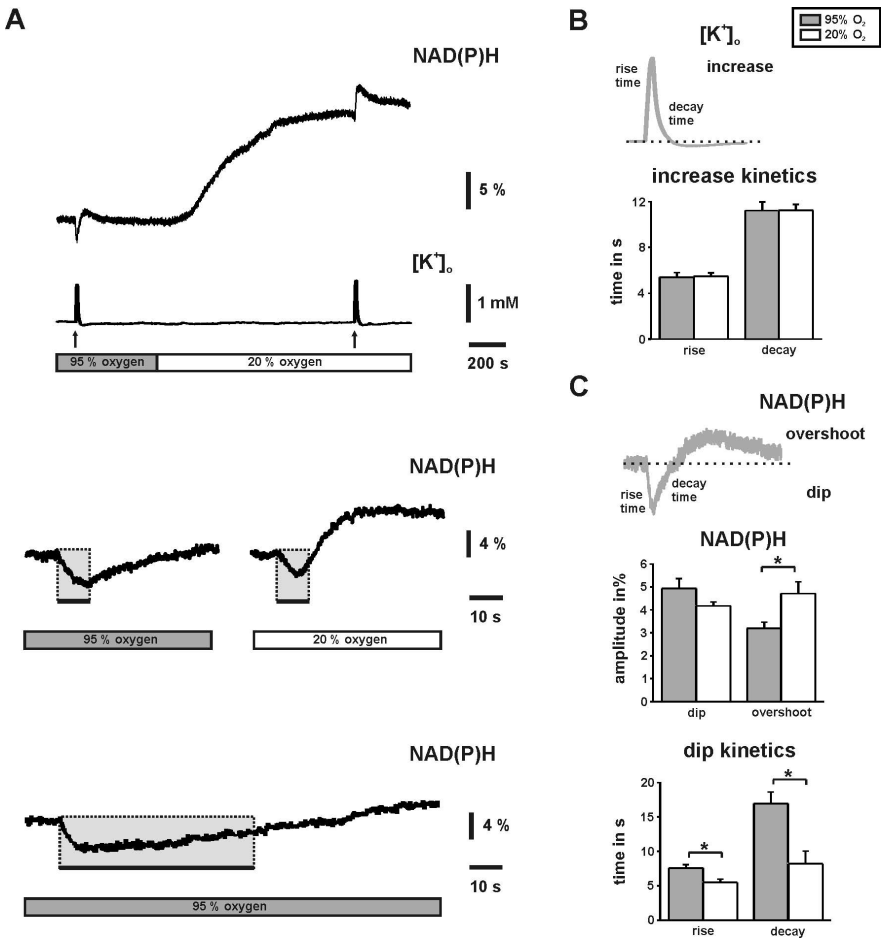

Figure 4. Changes in NAD(P)H fluorescence and $[K^+]_o$ in CA3. ***A***, The substantial NAD(P)H baseline elevation at 20% O_2 indicates reduced oxidation of the dinucleotide pools. Brief stimulus trains (10 s, 20 Hz; black arrows and bars) elicited biphasic NAD(P)H transients with different shapes under both oxygenation conditions (gray and white bars). The traces in the middle are from another experiment and displayed on an enlarged time scale. At 20% O_2, the biphasic NAD(P)H transient is characterized by a briefer initial "dip" component (gray rectangles) and a more rapidly developing and pronounced "overshoot" component. Note that the dip component terminates before the end of the stimulus train (right black bar). The bottom trace illustrates a NAD(P)H transient during a stimulus train of 60 s (20 Hz). ***B***, Pairs of stimulus-evoked transient increases in $[K^+]_o$ ($n = 8$) (***A***, $[K^+]_o$ trace) were analyzed for amplitudes (see Results) and kinetics (illustrated in scheme). Rise and decay times are given for the 10–90% intervals. ***C***, Pairs of stimulus-evoked biphasic NAD(P)H transients ($n = 8$) [***A***, NAD(P)H trace] were analyzed for amplitudes of dip (given as positive value) and overshoot components as well as for dip kinetics (illustrated in scheme). Note that NAD(P)H originated as the sum of fluorescence from stratum pyramidale and radiatum and that $[K^+]_o$ was simultaneously recorded in stratum pyramidale to quantify neuronal activation. $^*p < 0.05$.

Neuronal activity and interstitial pO_2

Compared with the hippocampus *in vivo*, excitatory and inhibitory neurons as well as neuronal networks develop similarly in organotypic hippocampal slice cultures (De Simoni et al., 2003), which are thus capable of expressing cholinergically evoked gamma oscillations (Fischer et al., 2002). Here, we show that gamma oscillations were highly sensitive to decreases in pO_2 within the normoxic range, whereas evoked neuronal population responses were unaffected. Moreover, the same pO_2 values, which significantly affected spontaneous network activity, also clearly interfered with the mitochondrial redox state. During cholinergically evoked gamma oscillations, the synchrony of the CA3 network is determined by AMPA receptor-mediated excitation and to a large extent by fast $GABA_A$ receptor-mediated inhibition (Fisahn et al., 1998; Mann et al., 2005; Bartos et al., 2007). Importantly, pyramidal cells generate action potentials at 1–3 Hz during both gamma oscillations and spontaneous network activity *in vitro* and *in vivo* (Csicsvari et al., 2003; Hájos et al., 2004; Sasaki et al., 2007). In contrast, fast-spiking interneurons fire action potentials up to 40 Hz in a phase-locked manner during gamma oscillations (Bragin et al., 1995; Hájos et al., 2004). Interestingly, several subtypes of fast-spiking interneurons express high levels of cytochrome *c*, suggesting substantial energy demand (Gulyás et al., 2006). Therefore, gamma oscillations appear to strongly depend on proper mitochondrial ATP and neurotransmitter formation to maintain both excitability and fast inhibition. Our data suggest that subtle decreases in pO_2 within the normoxic range weaken mitochondrial function and disturb the precise interplay of slow pyramidal cell and fast interneuron activities during gamma oscillations. This suggestion is supported by the pO_2 sensitivity of both slow- (<2 and 2–5 spikes/s) and fast (>5 spikes/s)-spiking neurons, the latter of which were ~10% in our recordings. According to estimates of ~12% nonpyramidal and mainly GABAergic neurons in the hippocampus (Caeser and Aertsen, 1991), both neuronal populations might represent pyramidal cells and interneurons, respectively. The pO_2 effect on slow- and fast-spiking neurons also indicated a persistent homeostasis between excitation and inhibition and might explain why we observed neither abnormal neuronal population responses nor a switch to pathological activity. However, because of the significant contribution of fast inhibition to generation of gamma oscillations, fast-spiking interneurons might be a critical target of alterations in pO_2 and mitochondrial function (Ackermann et al., 1984; Fuchs et al., 2007).

Strikingly, spontaneous network activity was already decreased at 20% O_2, whereas the interstitial pO_2 was still in the upper range of values (15–60 mmHg) as obtained in air-respiring rodents (Feng et al., 1988; Rolett et al., 2000; Erecinska and Silver, 2001; Takano et al., 2007). Moreover, the "critical" pO_2 for breakdown of steady-state aerobic metabolism has been reported between 7 and 9 mmHg (Rolett et al., 2000). However, it is difficult to compare our data with these studies because the *in vivo* recordings were made mainly in the cerebral cortex, partially with different techniques, and, notably, in the presence of anesthetics

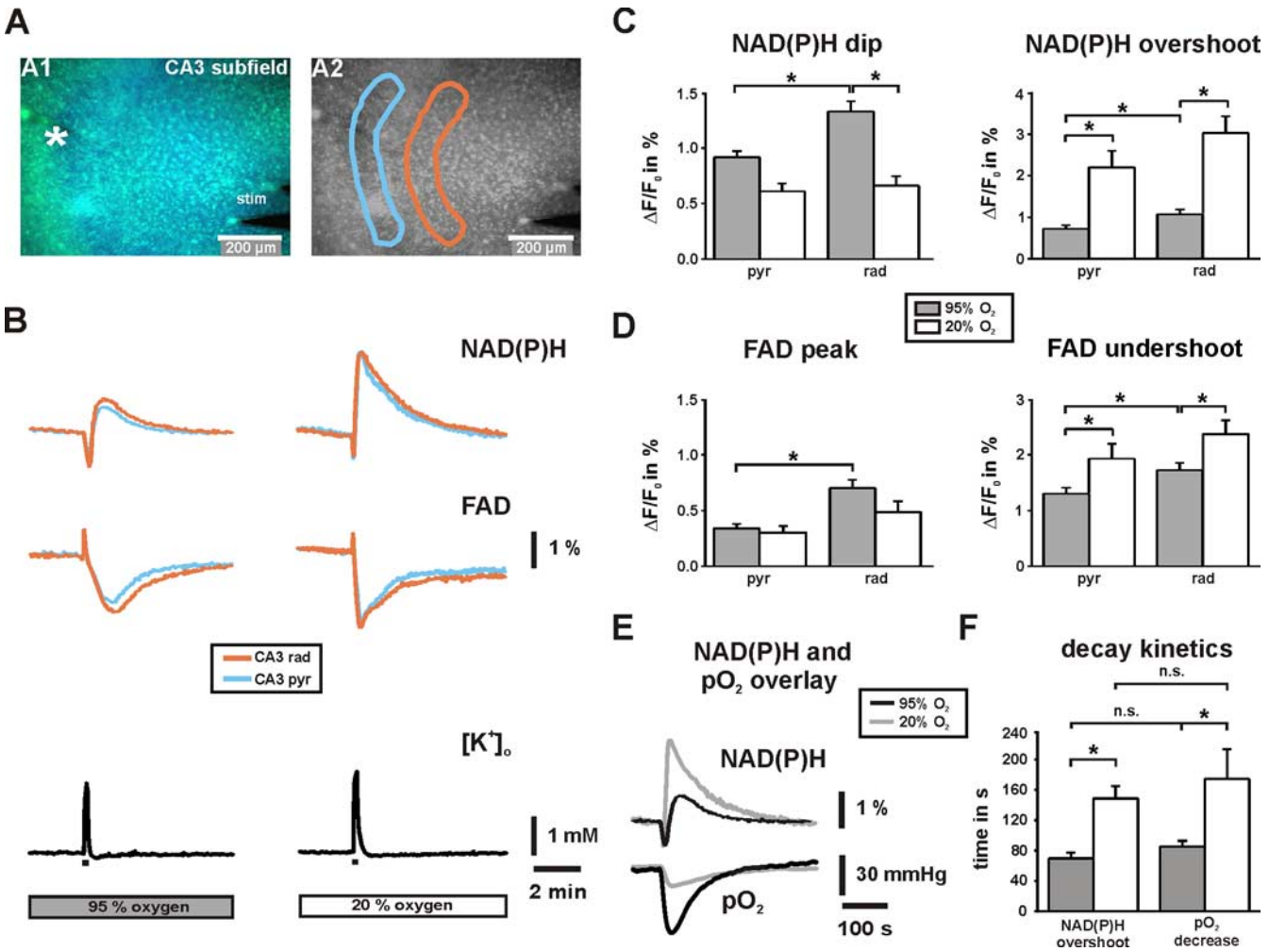

Figure 5. NAD(P)H and FAD fluorescence transients in stratum pyramidale and stratum radiatum in CA3. ***A***, Overlay of NAD(P)H and FAD fluorescence images as recorded with a delay of 130 ms. The K^+-sensitive electrode was positioned in stratum pyramidale (white asterisk), the bipolar stimulation electrode close to the dentate gyrus (stim) for electrical activation of fiber tracts to CA3. Regions of interests (light blue, stratum pyramidale; orange, stratum radiatum) were selected to determine changes in $\%\Delta F/F_0$ from image stacks that were recorded at 0.5 Hz. ***B***, The shapes of biphasic NAD(P)H (top traces) and FAD (middle traces) fluorescence transients as evoked by stimulus trains (10 s, 20 Hz; black bars) are clearly distinct at 20% O_2. Note that FAD transients (peak and undershoot) are inverse to NAD(P)H transients (dip and overshoot) because of different fluorescence properties of the dinucleotides. Transient increases in $[K^+]_o$ as evoked by stimulus trains were simultaneously recorded (bottom traces) and indicate virtually the same degree of neuronal activation at 95 and 20% O_2 (2.1 ± 0.1 and 2.4 ± 0.2 mM; $n = 18$; $p = 0.26$). ***C***, ***D***, Histograms summarizing the analysis of NAD(P)H and FAD transients ($n = 18$ each) in stratum pyramidale (pyr) and stratum radiatum (rad). Note that differences are most prominent in stratum radiatum. ***E***, Overlay of NAD(P)H and pO_2 transients in stratum pyramidale as evoked by stimulus trains. ***F***, Histogram summarizing the decay time constants of NAD(P)H overshoots and pO_2 transients at 95 and 20% O_2 ($n = 18$). *$p < 0.05$.

that can significantly interfere with both network oscillations and mitochondrial function (Whittington et al., 2000; Muravchick and Levy, 2006). In our study, the high sensitivity of gamma oscillations to changes in pO_2 and mitochondrial redox state might reflect effects on intrinsic membrane properties and/or synaptic transmission. Putative candidates are increased conductance of ATP-dependent K^+ channels (Fujimura et al., 1997), which might slightly hyperpolarize neurons from a critical membrane potential, amplification of activity-dependent neuronal acidification as a result of lactic acid production (Stenkamp et al., 2001), and alterations of glutamate/GABA metabolism and vesicle mobilization (Waagepetersen et al., 1999, Verstreken et al., 2005). It is important to stress that such abnormal processes might particularly occur in presynaptic and postsynaptic structures with high ion fluxes and energy demand, which critically rely on proper mitochondrial function and O_2 supply (Attwell and Iadecola, 2002). Such abnormal processes might be also aggravated during pathological processes like arteriosclerosis and neurodegenerative diseases, resulting in devastating disturbances of higher brain functions. Our data strongly suggest that the pO_2 threshold for robust gamma oscillations and spontaneous network activity is clearly above the "critical" value that has been reported to evoke neuronal depolarization and spreading depression as a result of generalized energy failure (Rolett et al., 2000; Foster et al., 2005). This suggestion is supported by an *in vivo* report demonstrating a tight correlation between synchronized gamma oscillations and hemodynamic signals in the visual cortex (Niessing et al., 2005), which might reflect an increased energy demand during gamma oscillations.

Stimulus-evoked neuronal activation and O_2 consumption

We show that neuronal activation as evoked by electrical stimulus trains was associated with rapid decreases in pO_2, reflecting enhanced mitochondrial O_2 consumption (Foster et al., 2005; Hayakawa et al., 2005). Interestingly, such pO_2 transients were significantly reduced and less variable at 20% O_2 compared with

hyperoxic conditions (95% O_2), which might indicate a significant reduction in O_2 availability at lower pO_2 (Foster et al., 2005). Alternatively, there might be a reduced efficacy of O_2 consumption at high pO_2, perhaps because of respiratory uncoupling (Andrews et al., 2005). During stimulation at 20% O_2, the pO_2 transiently dropped to 24.9 ± 2 mmHg, which was in the normoxic range. Nevertheless, we assume that this value might have been significantly lower in neuronal microdomains with high metabolic turnover (Jones, 1986; Erecinska and Silver, 2001; Attwell and Iadecola, 2002), which cannot be resolved with present available O_2 sensor techniques. This assumption is supported by our observation of smaller stimulus-evoked pO_2 transients at 20% O_2 that were associated with stronger alterations of mitochondrial redox responses in the synaptic compartment (stratum radiatum). In this context, it is important to note that proper mitochondrial function relies on a steep gradient of O_2 to overcome its low diffusion velocity in tissue. Further studies might clarify whether neuronal network oscillations are associated with transient local hypoxia in areas with high density of respiring mitochondria such as presynaptic and postsynaptic structures (Jones, 1986; Wong-Riley, 1989; Erecinska and Silver, 2001). Stimulus-evoked pO_2 transients also showed a slow recovery, particularly when recordings were made at lower pO_2. These observations likely reflect greater diffusion distances in slice preparations (~90–200 μm) compared with distances of ~25 μm from capillaries to neurons *in vivo* and, in addition, a reduced O_2 gradient from the surface to the slice core at 20% O_2 (Tata and Anderson, 2002; Turner et al., 2007).

We note that the prominent, stimulus-evoked decreases in pO_2 as observed in our slice preparation have been reported *in vivo* only under exceptional conditions, i.e., during cortical spreading depression (Takano et al., 2007) that is associated with a vasoconstriction in mice (Ayata et al., 2004), during electrical stimulation in the cerebellum, and when adaptations in blood flow are blocked (Offenhauser et al., 2005). Typically, neuronal activation *in vivo* is associated with a local rise in cerebral blood flow within a few seconds that markedly increases O_2 availability in the tissue. This process counteracts activity-dependent oxygen consumption and is reflected by biphasic changes in interstitial pO_2, namely a brief initial "dip" and an accentuated "overshoot" (Ances et al., 2001; Masamoto et al., 2003; Offenhauser et al., 2005).

Effects of interstitial pO_2 on mitochondrial redox state

We demonstrate that mitochondrial redox state and pO_2 are tightly coupled over a wide range of tissue oxygenation levels. At hyperoxic pO_2 (95% O_2), nicotinamide adenine and flavin adenine dinucleotide pools might have been overly oxidized to a certain degree (Mayevsky and Chance, 2007). Nevertheless, prominent initial dips of NAD(P)H transients (peaks of FAD transients) during electrical stimulation revealed a high oxidative capacity in the tissue at hyperoxic pO_2. Moreover, stimulus-evoked NAD(P)H transients at 95% O_2 were similar to those observed in the cortex *in vivo*, where sustained neuronal activation is associated with large NAD(P)H dips (Jöbsis et al., 1971; Mayevsky and Chance, 1975; LaManna et al., 1984), indicating that O_2 supply to the brain parenchyma is rapidly increased and allows enhanced mitochondrial electron transfer. In contrast, lowering interstitial pO_2 to 51 mmHg (20% O_2) markedly elevated NAD(P)H fluorescence and was associated with alterations of stimulus-evoked redox responses. Interestingly, similar but more pronounced alterations of evoked NAD(P)H transients were reported under hypoxic conditions *in vivo* (LaManna et al., 1984). These observations might argue for a reduced oxidative capacity of the mitochondrial electron transport chain at 20% O_2, which is also suggestive for a transient limitation of complex mitochondrial functions like ATP production, Ca^{2+} handling, and neurotransmitter formation (Waagepetersen et al., 1999; Kann and Kovács, 2007). In line with the discussion of pO_2 levels, a reduced mitochondrial oxidative capacity might particularly occur in neuronal microdomains with high metabolic turnover like synaptic compartments at 20% O_2. This assumption is supported by our data showing that redox responses as evoked in stratum radiatum are more sensitive to decreases in pO_2. Therefore, we propose that the effects of lower pO_2 on gamma oscillations and spontaneous network activity were primarily mediated by alterations of the mitochondrial redox state.

Our fluorescence data also provide an explanation for the discrepancies of NAD(P)H fluorescence recordings in different experimental models, because in contrast to *in vivo* recordings (Rosenthal and Jöbsis, 1971; Mayevsky and Chance, 1975; LaManna et al., 1984; Rex et al., 1999), the overshoot component dominates to a variable degree in acute and organotypic slice preparations (Lipton, 1973a; Kann et al., 2003; Shuttleworth et al., 2003). We propose that these discrepancies can be widely but not exclusively (see below) explained by interstitial pO_2 levels and greater diffusion distances in slice preparations, which critically determine mitochondrial oxidative capacity (see also Turner et al., 2007). Strikingly, we also demonstrate that cholinergically evoked gamma oscillations caused long-lasting NAD(P)H overshoots, although the interstitial pO_2 was clearly hyperoxic. At present, we cannot nominate the mechanisms underlying this kind of redox response. It might reflect an increase in substrate availability as a result of enhanced glycolysis in neuronal and astrocytic compartments (Kasischke et al., 2004; Brennan et al., 2006; Hertz et al., 2007), an imbalance of neuronal TCA cycle and mitochondrial electron transport chain activities, and/or the partial inhibition of the electron transport chain by free radicals (Brown, 2001; Erecinska and Silver, 2001). We also demonstrate that mitochondrial redox responses as evoked by gamma oscillations and stimulus trains at 95% O_2 were larger in the synaptic compartment (stratum radiatum). This likely reflects a higher metabolic demand of presynaptic and postsynaptic structures and perhaps increased enzyme activities and/or mitochondrial density (Wong-Riley, 1989; Waagepetersen et al., 1999; Attwell and Iadecola, 2002). Moreover, NAD(P)H and FAD transients showed a higher sensitivity to changes in pO_2 in the synaptic compartment, which might imply an enhanced vulnerability during pathological processes in hemodynamics and/or mitochondrial function.

Functional consequences and clinical aspects

We propose that even moderate decreases in pO_2 and/or mitochondrial dysfunction per se lead to significant disturbances of neuronal network activity. This might explain rapid loss of consciousness and occurrence of electroencephalographic slow-wave activity during brain ischemia, whereas evoked responses and ion distributions are more resistant (Hansen, 1985; Howard et al., 1998). Moreover, limitations of O_2 availability and mitochondrial dysfunction might occur locally during aging and in a variety of pathologies like arteriosclerosis, neurodegenerative diseases, epilepsy, or schizophrenia, which might significantly contribute to disturbances of higher brain functions in neurologic and psychiatric patients (Whittington et al., 2000; Kann et al., 2005; Vreugdenhil and Toescu, 2005; Cho et al., 2006). Our study highlights the importance of a functional understanding of

mitochondria and their implications on activities of individual neurons and neuronal networks in health and disease.

References

Ackermann RF, Finch DM, Babb TL, Engel Jr J (1984) Increased glucose metabolism during long-duration recurrent inhibition of hippocampal pyramidal cells. J Neurosci 4:251–264.

Amzica F, Steriade M (2000) Neuronal and glial membrane potentials during sleep and paroxysmal oscillations in the neocortex. J Neurosci 20:6648–6665.

Ances BM, Buerk DG, Greenberg JH, Detre JA (2001) Temporal dynamics of the partial pressure of brain tissue oxygen during functional forepaw stimulation in rats. Neurosci Lett 306:106–110.

Andrews ZB, Diano S, Horvath TL (2005) Mitochondrial uncoupling proteins in the CNS: in support of function and survival. Nat Rev Neurosci 6:829–840.

Attwell D, Iadecola C (2002) The neural basis of functional brain imaging signals. Trends Neurosci 25:621–625.

Ayata C, Shin HK, Salomone S, Ozdemir-Gursoy Y, Boas DA, Dunn AK, Moskowitz MA (2004) Pronounced hypoperfusion during spreading depression in mouse cortex. J Cereb Blood Flow Metab 24:1172–1182.

Bartos M, Vida I, Jonas P (2007) Synaptic mechanisms of synchronized gamma oscillations in inhibitory interneuron networks. Nat Rev Neurosci 8:45–56.

Bragin A, Jando G, Nadasdy Z, Hetke J, Wise K, Buzsáki G (1995) Gamma (40–100 Hz) oscillation in the hippocampus of the behaving rat. J Neurosci 15:47–60.

Brennan AM, Connor JA, Shuttleworth CW (2006) NAD(P)H fluorescence transients after synaptic activity in brain slices: predominant role of mitochondrial function. J Cereb Blood Flow Metab 26:1389–1406.

Brown GC (2001) Regulation of mitochondrial respiration by nitric oxide inhibition of cytochrome c oxidase. Biochim Biophys Acta 1504:46–57.

Buchheim K, Weissinger F, Siegmund H, Holtkamp M, Schuchmann S, Meierkord H (2002) Intrinsic optical imaging reveals regionally different manifestation of spreading depression in hippocampal and entorhinal structures in vitro. Exp Neurol 175:76–86.

Buzsáki G, Draguhn A (2004) Neuronal oscillations in cortical networks. Science 304:1926–1929.

Caeser M, Aertsen A (1991) Morphological organization of rat hippocampal slice cultures. J Comp Neurol 307:87–106.

Cho RY, Konecky RO, Carter CS (2006) Impairments in frontal cortical gamma synchrony and cognitive control in schizophrenia. Proc Natl Acad Sci USA 103:19878–19883.

Csicsvari J, Jamieson B, Wise KD, Buzsáki G (2003) Mechanisms of gamma oscillations in the hippocampus of the behaving rat. Neuron 37:311–322.

De Simoni A, Griesinger CB, Edwards FA (2003) Development of rat CA1 neurones in acute versus organotypic slices: role of experience in synaptic morphology and activity. J Physiol (Lond) 550:135–147.

Erecinska M, Silver IA (2001) Tissue oxygen tension and brain sensitivity to hypoxia. Respir Physiol 128:263–276.

Feng ZC, Roberts Jr EL, Sick TJ, Rosenthal M (1988) Depth profile of local oxygen tension and blood flow in rat cerebral cortex, white matter and hippocampus. Brain Res 445:280–288.

Fisahn A, Pike FG, Buhl EH, Paulsen O (1998) Cholinergic induction of network oscillations at 40 Hz in the hippocampus in vitro. Nature 394:186–189.

Fischer Y, Wittner L, Freund TF, Gahwiler BH (2002) Simultaneous activation of gamma and theta network oscillations in rat hippocampal slice cultures. J Physiol (Lond) 539:857–868.

Foster KA, Beaver CJ, Turner DA (2005) Interaction between tissue oxygen tension and NADH imaging during synaptic stimulation and hypoxia in rat hippocampal slices. Neuroscience 132:645–657.

Fuchs EC, Zivkovic AR, Cunningham MO, Middleton S, Lebeau FE, Bannerman DM, Rozov A, Whittington MA, Traub RD, Rawlins JN, Monyer H (2007) Recruitment of parvalbumin-positive interneurons determines hippocampal function and associated behavior. Neuron 53:591–604.

Fujimura N, Tanaka E, Yamamoto S, Shigemori M, Higashi H (1997) Contribution of ATP-sensitive potassium channels to hypoxic hyperpolarization in rat hippocampal CA1 neurons in vitro. J Neurophysiol 77:378–385.

Gaedicke R, Albus K (1995) Real-time separation of multineuron recordings with a DSP32C signal processor. J Neurosci Methods 57:187–193.

Gulyás AI, Buzsáki G, Freund TF, Hirase H (2006) Populations of hippocampal inhibitory neurons express different levels of cytochrome c. Eur J Neurosci 23:2581–2594.

Hájos N, Palhalmi J, Mann EO, Nemeth B, Paulsen O, Freund TF (2004) Spike timing of distinct types of GABAergic interneuron during hippocampal gamma oscillations *in vitro*. J Neurosci 24:9127–9137.

Hansen AJ (1985) Effect of anoxia on ion distribution in the brain. Physiol Rev 65:101–148.

Hayakawa Y, Nemoto T, Iino M, Kasai H (2005) Rapid Ca^{2+}-dependent increase in oxygen consumption by mitochondria in single mammalian central neurons. Cell Calcium 37:359–370.

Heinemann U, Arens J (1992) Production and calibration of ion-sensitive microelectrodes. In: Practical electrophysiological methods (Kettenmann H, Grantyn R, eds), pp 206–212. New York: Wiley.

Heinemann U, Schaible HG, Schmidt RF (1990) Changes in extracellular potassium concentration in cat spinal cord in response to innocuous and noxious stimulation of legs with healthy and inflamed knee joints. Exp Brain Res 79:283–292.

Hertz L, Peng L, Dienel GA (2007) Energy metabolism in astrocytes: high rate of oxidative metabolism and spatiotemporal dependence on glycolysis/glycogenolysis. J Cereb Blood Flow Metab 27:219–249.

Howard EM, Gao TM, Pulsinelli WA, Xu ZC (1998) Electrophysiological changes of CA3 neurons and dentate granule cells following transient forebrain ischemia. Brain Res 798:109–118.

Huang S, Heikal AA, Webb WW (2002) Two-photon fluorescence spectroscopy and microscopy of NAD(P)H and flavoprotein. Biophys J 82:2811–2825.

Jöbsis FF, O'Connor M, Vitale A, Vreman H (1971) Intracellular redox changes in functioning cerebral cortex. I. Metabolic effects of epileptiform activity. J Neurophysiol 34:735–749.

Jones DP (1986) Intracellular diffusion gradients of O2 and ATP. Am J Physiol 250:663–675.

Kann O, Kovács R (2007) Mitochondria and neuronal activity. Am J Physiol Cell Physiol 292:C641–C657.

Kann O, Schuchmann S, Buchheim K, Heinemann U (2003) Coupling of neuronal activity and mitochondrial metabolism as revealed by NAD(P)H fluorescence signals in organotypic hippocampal slice cultures of the rat. Neuroscience 119:87–100.

Kann O, Kovács R, Njunting M, Behrens CJ, Otáhal J, Lehmann TN, Gabriel S, Heinemann U (2005) Metabolic dysfunction during neuronal activation in the ex vivo hippocampus from chronic epileptic rats and humans. Brain 128:2396–2407.

Kasischke KA, Vishwasrao HD, Fisher PJ, Zipfel WR, Webb WW (2004) Neural activity triggers neuronal oxidative metabolism followed by astrocytic glycolysis. Science 305:99–103.

Kunz WS, Kunz W (1985) Contribution of different enzymes to flavoprotein fluorescence of isolated rat liver mitochondria. Biochim Biophys Acta 841:237–246.

LaManna JC, Light AI, Peretsman SJ, Rosenthal M (1984) Oxygen insufficiency during hypoxic hypoxia in rat brain cortex. Brain Res 293:313–318.

Lipton P (1973a) Effects of membrane depolarization on nicotinamide nucleotide fluorescence in brain slices. Biochem J 136:999–1009.

Lipton P (1973b) Effects of membrane depolarization on light scattering by cerebral cortical slices. J Physiol (Lond) 231:365–383.

Lisman JE, Idiart MA (1995) Storage of 7 +/- 2 short-term memories in oscillatory subcycles. Science 267:1512–1515.

Mann EO, Suckling JM, Hájos N, Greenfield SA, Paulsen O (2005) Perisomatic feedback inhibition underlies cholinergically induced fast network oscillations in the rat hippocampus in vitro. Neuron 45:105–117.

Masamoto K, Omura T, Takizawa N, Kobayashi H, Katura T, Maki A, Kawaguchi H, Tanishita K (2003) Biphasic changes in tissue partial pressure of oxygen closely related to localized neural activity in guinea pig auditory cortex. J Cereb Blood Flow Metab 23:1075–1084.

Mayevsky A, Chance B (1975) Metabolic responses of the awake cerebral cortex to anoxia hypoxia spreading depression and epileptiform activity. Brain Res 98:149–165.

Mayevsky A, Chance B (2007) Oxidation-reduction states of NADH in vivo: from animals to clinical use. Mitochondrion 7:330–339.

Montgomery SM, Buzsáki G (2007) Gamma oscillations dynamically couple hippocampal CA3 and CA1 regions during memory task performance. Proc Natl Acad Sci USA 104:14495–14500.

Muravchick S, Levy RJ (2006) Clinical implications of mitochondrial dysfunction. Anesthesiology 105:819–837.

Niessing J, Ebisch B, Schmidt KE, Niessing M, Singer W, Galuske RA (2005) Hemodynamic signals correlate tightly with synchronized gamma oscillations. Science 309:948–951.

Offenhauser N, Thomsen K, Caesar K, Lauritzen M (2005) Activity-induced tissue oxygenation changes in rat cerebellar cortex: interplay of postsynaptic activation and blood flow. J Physiol (Lond) 565:279–294.

Pomper JK, Haack S, Petzold GC, Buchheim K, Gabriel S, Hoffmann U, Heinemann U (2006) Repetitive spreading depression-like events result in cell damage in juvenile hippocampal slice cultures maintained in normoxia. J Neurophysiol 95:355–368.

Popov V, Medvedev NI, Davies HA, Stewart MG (2005) Mitochondria form a filamentous reticular network in hippocampal dendrites but are present as discrete bodies in axons: a three-dimensional ultrastructural study. J Comp Neurol 492:50–65.

Rex A, Pfeifer L, Fink F, Fink H (1999) Cortical NADH during pharmacological manipulations of the respiratory chain and spreading depression in vivo. J Neurosci Res 57:359–370.

Rolett EL, Azzawi A, Liu KJ, Yongbi MN, Swartz HM, Dunn JF (2000) Critical oxygen tension in rat brain: a combined (31)P-NMR and EPR oximetry study. Am J Physiol Regul Integr Comp Physiol 279:R9–R16.

Rosenthal M, Jöbsis FF (1971) Intracellular redox changes in functioning cerebral cortex. II. Effects of direct cortical stimulation. J Neurophysiol 34:750–762.

Sasaki T, Matsuki N, Ikegaya Y (2007) Metastability of active CA3 networks. J Neurosci 27:517–528.

Scholz R, Thurman RG, Williamson JR, Chance B, Bucher T (1969) Flavin and pyridine nucleotide oxidation-reduction changes in perfused rat liver. J Biol Chem 244:2317–2324.

Schuchmann S, Kovács R, Kann O, Heinemann U, Buchheim K (2001) Monitoring NAD(P)H autofluorescence to assess mitochondrial metabolic functions in rat hippocampal-entorhinal cortex slices. Brain Res Brain Res Protoc 7:267–276.

Shuttleworth CW, Brennan AM, Connor JA (2003) NAD(P)H fluorescence imaging of postsynaptic neuronal activation in murine hippocampal slices. J Neurosci 23:3196–3208.

Stenkamp K, Palva JM, Uusisaari M, Schuchmann S, Schmitz D, Heinemann U, Kaila K (2001) Enhanced temporal stability of cholinergic hippocampal gamma oscillations following respiratory alkalosis in vitro. J Neurophysiol 85:2063–2069.

Takano T, Tian GF, Peng W, Lou N, Lovatt D, Hansen AJ, Kasischke KA, Nedergaard M (2007) Cortical spreading depression causes and coincides with tissue hypoxia. Nat Neurosci 10:754–762.

Tata DA, Anderson BJ (2002) A new method for the investigation of capillary structure. J Neurosci Methods 113:199–206.

Thompson JK, Peterson MR, Freeman RD (2003) Single-neuron activity and tissue oxygenation in the cerebral cortex. Science 299:1070–1072.

Turner DA, Foster KA, Galeffi F, Somjen GG (2007) Differences in O_2 availability resolve the apparent discrepancies in metabolic intrinsic optical signals in vivo and in vitro. Trends Neurosci 30:390–398.

Verstreken P, Ly CV, Venken KJ, Koh TW, Zhou Y, Bellen HJ (2005) Synaptic mitochondria are critical for mobilization of reserve pool vesicles at *Drosophila* neuromuscular junctions. Neuron 47:365–378.

Vreugdenhil M, Toescu EC (2005) Age-dependent reduction of gamma oscillations in the mouse hippocampus in vitro. Neuroscience 132:1151–1157.

Waagepetersen HS, Sonnewald U, Schousboe A (1999) The GABA paradox: multiple roles as metabolite, neurotransmitter, and neurodifferentiative agent. J Neurochem 73:1335–1342.

Whittington MA, Faulkner HJ, Doheny HC, Traub RD (2000) Neuronal fast oscillations as a target site for psychoactive drugs. Pharmacol Ther 86:171–190.

Wong-Riley MT (1989) Cytochrome oxidase: an endogenous metabolic marker for neuronal activity. Trends Neurosci 12:94–101.